Chapter 8
Evaluation of Submarine Groundwater Discharge as a Coastal Nutrient Source and Its Role in Coastal Groundwater Quality and Quantity

Henrietta Dulai, Alana Kleven, Kathleen Ruttenberg, Rebecca Briggs, and Florence Thomas

Abstract Globally, submarine groundwater discharge (SGD) is responsible for 3–4 times the water discharge delivered to the oceans by rivers. Moreover, nutrient concentrations in SGD are usually elevated in comparison to river fluxes. Here we review the major advances in the field of SGD studies and related nutrient fluxes to the coastal ocean. To demonstrate the significance of SGD as terrestrial nutrient pathway we compare stream and submarine groundwater discharge rates in a watershed on the windward side of Oahu, one of the major islands of the Hawaii archipelago. Our analysis of Kaneohe Bay, which hosts the largest coral reefs on the island revealed that SGD in the form of total (fresh+brackish) groundwater discharge was 2–4 times larger than surface inputs. Corresponding DIN and silicate fluxes were also dominated by SGD, while DIP was delivered mostly via streams. We quantified bulk nutrient uptake in coastal waters and also demonstrated that nutrients were quickly removed from the bay due to fast coastal flushing rates. This study demonstrates the need to understand SGD-derived nutrient fluxes in order to evaluate land-based coastal nutrient and pollution sources.

H. Dulai (✉) • A. Kleven
Department of Geology and Geophysics, University of Hawaii-Manoa, Honolulu, HI, USA
e-mail: hdulaiov@hawaii.edu

K. Ruttenberg
Department of Geology and Geophysics, University of Hawaii-Manoa, Honolulu, HI, USA

Department of Oceanography, University of Hawaii-Manoa, Honolulu, HI, USA

R. Briggs
Department of Oceanography, University of Hawaii-Manoa, Honolulu, HI, USA

F. Thomas
Hawaii Institute of Marne Biology, University of Hawaii-Manoa, Honolulu, HI, USA

Abbreviations

A_{Rn_cw}	Coastal water radon activity
A_{Rn_gw}	Groundwater radon activity
C_T	Terrestrial nutrient concentration
CB	Central Kaneohe Bay
CI	Coconut Island
DIN	Dissolved inorganic nitrogen
DIP	Dissolved inorganic phosphorus
DON	Dissolved organic nitrogen
DOP	Dissolved organic phosphorus
dpm	Decays per minute
GPS	Global positioning system
gw	Groundwater
HFP	Heeia Fishpond
I	Effective terrestrial end-member nutrient concentration
K_h	Horizontal eddy diffusion coefficient
L	Length
n	Number
NB	Northwest Kaneohe Bay
Q_T	Terrestrial water flux
Q_{SGD}	Submarine groundwater discharge flux
R	Nutrient removal rate
Ra	Radium
Ra_i	Nearshore water radium activity
Ra_o	Offshore water radium activity
Rn	Radon
SGD	Submarine groundwater discharge
STE	Subterranean estuary
sw	Surface water
t	Time, residence time, flushing rate
$T_{1/2}$	Radionuclide half-life
T1	Transect 1
T2	Transect 2
T3	Transect 3
TDN	Total dissolved nitrogen
TDP	Total dissolved phosphorus
Th	Thorium
U	Uranium
V	Volume
λ	Radionuclide decay constant

1   Introduction

1.1   SGD: General Description

Submarine groundwater discharge (SGD) consists of fresh meteoric water and recirculated seawater that flows through the coastal aquifer into coastal waters (Taniguchi et al. 2002). Most often it emerges as a mixture of fresh and saline water masses resulting in a full salinity range (Michael et al. 2005; Santos et al. 2012; Gonneea and Charette 2014). Generally elevated SGD is associated with certain characteristics of coastlines such as steep topography with permeable geology and high rainfall (Bokuniewicz et al. 2003). However, groundwater fluxes have been identified on all seven continents and can occur under non-typical conditions. For example, prolific meteoric water discharge has been found associated with otherwise desert-like watersheds (Johnson et al. 2008), seeping inconspicuously under estuaries (Moore 1997; Dulaiova et al. 2006; Peterson et al. 2009; Wang et al. 2014) and on coastlines with absent freshwater fluxes dominated by seawater recirculation (Kiro et al. 2013).

Based on coastal hydrological principles, SGD distribution in a cross-shore direction is expected to decrease exponentially with increasing distance offshore (Taniguchi et al. 2003). The presence of confining layers however, allows water discharge to occur kilometers from shorelines and at significant ocean depths (Moore and Wilson 2005). The majority of reported SGD studies have been performed in shallow coastal regions where its impact is the most significant in terms of pollution. Here the SGD signature is magnified by less dilution due to lesser water volumes and longer coastal residence times. As a consequence, the literature is biased towards SGD in the nearshore region (Bratton 2010).

The focus of SGD studies has diverged in multiple directions, including hydrological, geochemical, ecological, and coastal management aspects of SGD. Studies of biogeochemical processes in the subterranean estuary (STE), a subsurface zone of mixing between fresh groundwater and recirculated seawater (Moore 1999), helped to explain the composition of discharging fluids influenced by nutrient transformations (Kroeger and Charette 2008; Santos et al. 2008, Kim et al. 2012), trace metal cycling (Charette et al. 2005; Beck et al. 2009, 2013; Gonneea et al. 2008), and microbial activity (Santoro et al. 2006) in the STE. It has become clear that groundwater geochemical signatures undergo significant changes in the STE just before discharging into the coastal zone. There has also been progress in the understanding and description of terrestrial and marine driving forces of SGD (Michael et al. 2005; Robinson et al. 2006, 2007; Li and Jiao 2013; Gonneea et al. 2008). Gonneea and Charette (2014) illustrated that in addition to the terrestrial drivers such as precipitation and groundwater extraction, sea-level anomalies had a quantifiable effect on the magnitude and composition of SGD. Relevant to this marine forcing is the expected effect of the advancing sea level rise, which in addition to increased seawater intrusion is predicted to change biogeochemical interactions in the STE and may result in increased SGD solute

fluxes (e.g. Roy et al. 2010). While most of the early literature focused on nutrient (e.g. Slomp and Van Cappellen 2004; Andersen et al. 2007; Bowen and Valiela 2001) and trace metal SGD fluxes (e.g. Beck et al. 2009), there is an emerging trend of a more interdisciplinary focus on SGD and its ecological consequences, including ocean acidification and its effect on coral reefs (Cyronak et al. 2014; Santos et al. 2013), linking SGD nutrient inputs to enhanced primary productivity (Waska and Kim 2011) and algal proliferation leading to coral reef degradation (Dailer et al. 2010; Smith et al. 2001).

1.2 SGD-Derived Nutrient Fluxes

Total SGD consists of meteoric fresh groundwater, which is responsible for supplying allochthonous, new terrestrial nutrients to the coastal zone, and recirculated seawater, which either carries nutrients with it from the sea or acquires them as the water flows through the STE and the seabed. Local remineralization of marine organic matter is the origin of nutrients in the latter case, which is not considered a new but an autochthonous nutrient source to the coastal waters; it is still significant, however, because it mobilizes recycled nutrients. Upon exiting the STE, the fate of SGD-derived coastal nutrients is analogous to those in river estuaries in that one may expect the same chemical continuity between groundwater and ocean water as in estuaries. Therefore it is evident that nutrients are being processed through two estuaries, once in the subsurface (the STE) and once on the surface where brackish groundwater plumes mix into the coastal water.

Nutrient fluxes are estimated by quantification of SGD (Moore 2010) and by multiplication of the water discharge by STE nutrient concentrations. This approach requires the assumption that no nutrient uptake processes or sources occur between the STE and the SGD discharge point. But as Moore (2010) points out, while SGD is relatively easy to quantify, constituent fluxes within the STE are so variable that the largest uncertainties in SGD-derived nutrient fluxes stem from the determination of the proper solute nutrient end-member. The most commonly used methods of SGD assessments are geochemical tracer techniques (Charette et al. 2008), thermal imaging (Johnson et al. 2008), geophysical techniques (Dimova et al. 2012), hydrological and watershed models (Gonneea and Charette 2014), and direct measurements using seepage meters (Lee 1977).

In the simplest scenario there is conservative mixing between groundwater nutrients and seawater resulting in a linear trend of nutrients with either salinity (Knee et al. 2010) or a groundwater tracer (Moore 2006) across the STE. This approach assumes that the recirculated seawater is nutrient-poor, and its role in the STE is mainly as a dilution agent. Typically there would also be a limited amount of organic matter remineralization within the STE, resulting in the absence of added recycled nutrients. In this case the SGD-derived nutrient flux is simply the product of fresh SGD and freshwater nutrient concentrations (Knee et al. 2010).

In more complex STE settings various nitrogen attenuation processes have been described with concurrent removal of nitrate and ammonium (Kroeger and Charette 2008; Santos et al. 2010, 2012; Glenn et al. 2013). As a result, SGD has lower nitrogen concentrations than the terrestrial end-member upstream of the STE. Similarly, reactive phosphate readily interacts with solids containing iron and aluminum oxides resulting in its removal and cycling within the STE (Spiteri et al. 2008). Gonneea and Charette (2014) reported a net removal of phosphate within the STE and a change of N:P ratios in terrestrial groundwater before and after flowing through the STE.

Nutrient additions may occur via seawater circulation through organic-rich benthic sediments. This addition is very typical for salt marshes where tidal pumping is one of the major nutrient recycling pathways (Weston et al. 2006; Wilson and Gardner 2006; Wankel et al. 2009). In several cases multiple SGD signatures have been found in the coastal zone suggesting discharges of different water masses with different nutrient compositions. Geochemical tracer balances have been used to identify and quantify these sources (Moore 2003; Charette 2007).

1.3   Nutrient Removal in the Coastal Zone

We can make an analogy between river estuaries and SGD plumes mixing into the coastal ocean. They are different in that estuaries are surficially-expressed, semi-enclosed bodies while SGD discharges along any type of coastline geometry— enclosed embayments as well as well-flushed coastal margins. They are similar, however, in that they are reaction vessels through which terrestrial solutes and solids must pass before entering the ocean (Kaul and Froelich 1984). It is therefore important to understand how SGD-derived nutrients are affected during their passage through the coastal ocean. In some instances nutrients are not stripped from SGD plumes because their transit time is too short with respect to phyto-plankton cell division times (Tomasky et al. 2013). In many examples, however, there is significant coastal biological uptake resulting in deviations from conservative estuarine mixing models analogous to those described in rivers (Kaul and Froelich 1984). For example, primary production sustained by SGD-derived nutrients has been documented to result in non-conservative nitrate and silicate mixing trends and a removal of 40–90 % of nutrients within the coastal zone of small islands (Kim et al. 2011).

1.4   Case Study of Coastal Nutrient Fluxes

In this paper we present a case study that demonstrates the combined use of the most commonly applied natural radioisotopic techniques using radon and radium isotopes (Charette et al. 2008). The derived SGD is then used to estimate corresponding nutrient fluxes.

Terrestrial nutrient fluxes are investigated in two parts of Kaneohe Bay, Hawaii. The first is in a section of a watershed where the STE is presumed to play very little role in nutrient removal and a conservative nutrient behavior is expected; the second is a region of the watershed where a coastal wetland significantly alters groundwater and stream nutrient concentrations just before these discharge into the ocean. We illustrate the significance of SGD for coastal nutrient budgets in Kaneohe Bay through the following steps:

– we compare nutrient fluxes via SGD to stream inputs in different sectors of the bay
– we estimate coastal nutrient inventories and coastal residence times
– we study the estuarine behavior of SGD-derived nutrients and estimate net nutrient removal rates.

Due to the unique island watershed characteristics described below, our study site is not typical for continental margins but is a good representative of large islands, which account for the majority of SGD inputs into the Pacific Ocean. On the downstream end of the watershed a coral reef along with associated native and invasive algal communities co-exist in a delicate nutrient balance. In addition, our study site includes a fishpond, built by early Hawaiians who recognized the parts of the coastline where ample nutrient delivery by streams and groundwater discharge could sustain a vibrant aquaculture. With population growth and increased anthropogenic nutrient and sediment fluxes, the pond and the coral reef have been threatened by euthrophication, excess sediment loads, and algal overgrowth. We illustrate that among the various nutrient delivery mechanisms SGD plays a pivotal role in these systems.

2 Methods

2.1 Study Site

The Kaneohe watershed is located on the northeast, windward side of Oahu, the third largest island of the Hawaiian archipelago. It consists of several stream-eroded, amphitheater-headed valleys with steep headwalls and alluvial deposits. The deposits are iron and aluminum rich clays with high affinity for phosphate, radium isotopes, and ammonium. Orographic rainfall is typical for all sectors of the steep watershed. Our study focused on the northwest part, which is divided into Waikane, Waiahole and Kaaawa/Hakipuu sub-watersheds (area 36 km^2, precipitation 2.6×10^5 m^3 d^{-1}, 55 % of watershed stream runoff) and Kaneohe (area 56 km^2, precipitation 3.6×10^5 m^3 d^{-1}, 39 % of watershed stream runoff) in the central sector of the bay (Shade and Nichols 1996). The watershed has high-level, dike impounded groundwater and a basal lens which is connected to the coastal zone. Land-use is agriculture and preservation land in the northwest, low-intensity developed and preservation in the central sector, with most urban development located

along the coastline and the southern part of the watershed. The coastal plain of the Heeia sector has a 0.81 km^2 wetland. Kaneohe bay is a semi-enclosed embayment with a barrier reef as a seaward boundary. In the lagoon there are patch reefs and fringing reefs, many of which have been substantially modified by the growth of fleshy algae. The fringing reef flats receive land-derived mud, sand, and rubble. The bottom sediments in the nearshore region are mostly noncalcareous clays, while sand bars and hard bottom are more typical outside of the lagoons (Smith et al. 1981).

We selected three shore-perpendicular transects (T1–T3) along fringing reefs in Kaneohe Bay (Fig. 8.1). The array of transects was selected based on specific characteristics of their location that we believed might influence the delivery of nutrients (Table 8.1). For example, Transects 2 in Waiahole and 3 in Kaaawa/ Hakipuu (T2 and T3) are located proximal to freshwater input via stream runoff. In contrast, Transect 1 in Waikane (T1), the northernmost transect, is located in a region with minimal input from surface runoff, and in the most pristine (lowest apparent anthropogenic impact) sector of the bay. Sampling locations in Central Bay (CB Fig. 8.1) only covered the northernmost tip of this subwatershed.
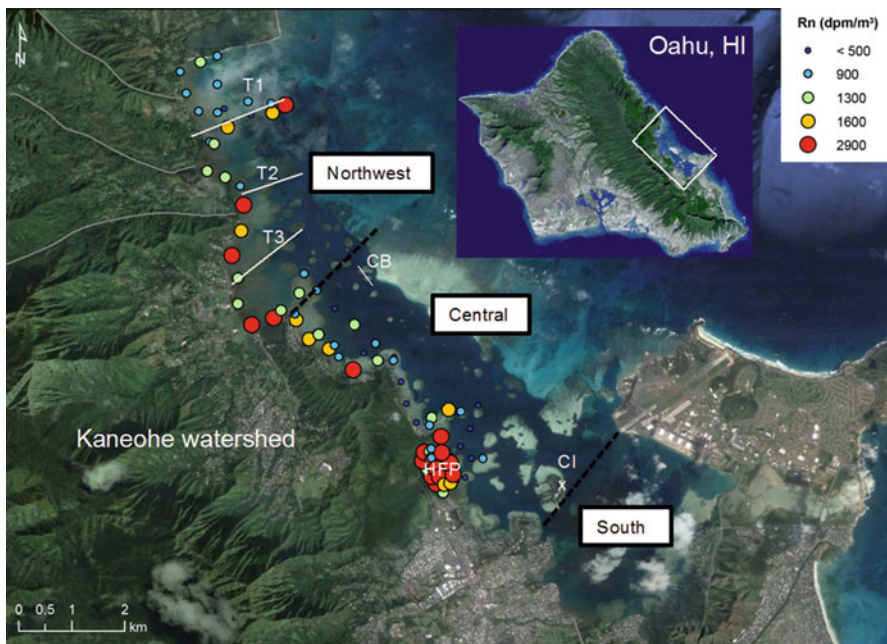

Fig. 8.1 Kaneohe Watershed is located on the windward side of Oahu, HI. The watershed consists of several sub-watersheds (divided by *grey lines*). Kaneohe Bay is composed of three sectors: northwest (NB), central (CB) and south. Radium samples were collected along transects T1–T3 in NB, at a location indicated by CB and in the Heeia Fishpond (HFP). Surface water radon activities (indicated by *colored circles*) were measured along the coastline in NB and CB as well as in HFP. Radon time-series monitoring was performed on Coconut Island (CI) located in the central sector of the bay

In our study we also included Heeia fishpond, which is a 0.39 km^2 walled estuary downstream of the Heeia wetland in the central sector of the bay. It receives water from the Heeia stream and the ocean through channels. It receives approximately 50 % of the stream flow measured at the Haiku stream gauge (USGS 16275000) (Young 2011). The pond is shallow, on average 0.5 m (Timmerman et al. 2015), and is used for aquaculture.

2.2 Radium Isotopic Sampling and Analysis

In order to quantify groundwater fluxes and nutrient distribution in the northwest sector of the bay, we examined three transects (T1–T3, Fig. 8.1) that extended from the coastline out to ocean salinities (2000–3000 m). In the central sector we collected only three samples at 2000 m from the shoreline (location CB, Fig. 8.1); these points were not aligned on a transect. Samples were collected in both sectors on August 17, 2010 during a dry period and in the northwest sector following the first big storm on November 4, 2010. Heeia fishpond was sampled on November 19, 2013, when we collected five samples that covered most representative salinity ranges across the pond. Surface water samples were collected into 20-L carboys for radium isotopic analysis, and for nutrient analysis (described below). Salinity was measured at the top and bottom of the water column at the time of sampling using a YSI multiparameter conductivity meter. Radium samples were weighed, filtered through MnO_2-coated acrylic fibers and analyzed on a Radium Delayed Coincidence Counter (Scientific Instruments) for short-lived ^{224}Ra, ^{223}Ra, and ^{228}Th. Excess ^{224}Ra was calculated by subtracting dissolved ^{228}Th activities before decay correction and all ^{224}Ra reported from here on refer to excess ^{224}Ra. ^{227}Ac was below detection limit of our method in all samples and all ^{223}Ra reported here is assumed to be excess ^{223}Ra. Long-lived ^{226}Ra and ^{228}Ra were measured on ashed fiber samples using a high purity germanium detector (Ortec, GEM40).

2.3 Surface Water Profiling and Nutrient Sampling

Water column temperature and salinity was profiled using a YSI 6200v Sonde, which was manually lowered off the side of the boat at a steady rate during constant data logging for a continuous profile of these parameters from surface to bottom water. Depth profiles were used to determine the surface mixed layer thickness by determining the depth at which salinities increased to offshore levels. Discrete water samples in the bay and fishpond were collected from surface waters and immediately transferred to shore for filtration. Nutrient samples were filtered through pre-weighed 0.2 μm polycarbonate filters and frozen until analysis. Nutrient samples from T1, T2, T3 were analyzed for dissolved PO_4^{3-}, $Si(OH)_4$, NO_3^-, NO_2^-, NH_4^+, total dissolved nitrogen (TDN), and total dissolved phosphorus (TDP) on a Technicon AutoAnalyzer II® following well-established analytical methods at the Water Center at the University of Washington. Water samples collected in 2012

from HFP were analyzed on a Seal Analytical AA3® following well-established analytical methods at the SOEST Laboratory for Analytical Biogeochemistry at the University of Hawaii. Dissolved organic phosphorus (DOP) and dissolved organic nitrogen (DON) were determined as the difference between TDP and TDN and the dissolved inorganic P and N pools.

2.4 Radon Survey

A surface water radon survey along the coastline, extending from the northernmost tip of the bay to the central-south sector boundary, was performed on August 17, 2010. The survey was done at high tide because the shallow parts of the reef were not accessible at low tide. We used an autonomous in situ radon detector (Rad-Aqua) into which water was pumped from about 0.2 m below water surface. The unit was housed on a dinghy moving at <5 km h^{-1} speed. A radon survey was also performed in Heeia fishpond on November 19, 2013 during which we followed the entire perimeter of the pond and a central transect in the pond covering most of the pond area. Salinity and GPS coordinates were recorded every 30 s along the surveys (Fig. 8.1). Radon data were processed using methods described in Dulaiova et al. (2010).

2.5 Radon Time Series

A 1-h resolution radon (Rn) time-series of Rn in surface waters off Coconut Island (Fig. 8.1) was set-up for the period of January 26, 2012 and March 22, 2012. Water from 0.2 m below surface was pumped into a Rad-Aqua instrument housed in a land-based structure. Salinity, temperature and wind speed was monitored along with the radon time-series. Radon data were processed using methods described in Burnett and Dulaiova (2003).

2.6 Wetland and Groundwater Sampling

We collected groundwater samples in the wetland using piezometers from 0.5 to 2.0 m depth and surface water from the stream and irrigation ditches. Groundwater samples in the upper watershed were collected from wells operated by the Board of Water Supply. Samples were analyzed for nutrients as described above and radon activities using a RAD-H2O system (Durridge Inc).

3 Results

3.1 Radium Isotope Distribution

In northwest Kaneohe Bay radium isotope enrichment was higher, in general, in the nearshore region (Fig. 8.2) although the long-lived ^{226}Ra had the opposite trend along T3, which was more pronounced in November 2010. We attribute this result to radium addition to the offshore section of the transect from nearby streams and/or removal in the nearshore water column by sorption to iron rich suspended particles (see below). Radium activities were 2–12 dpm m^{-3} ^{223}Ra, 2–45 dpm m^{-3} ^{224}Ra, and 20–160 dpm m^{-3} ^{226}Ra. In general the activities were higher in August than November 2010. Radium distribution against salinity showed that radium activities dropped significantly by the seaward end of the transects but have not reached ocean end-member levels of zero excess (Fig. 8.2). Salinities along these transects ranged from 17 to 35.7 and the water column was stratified reaching ocean salinities near the bottom.

Radium isotopes in the fishpond were 2–8 dpm m^{-3} ^{223}Ra, 13–40 dpm m^{-3} ^{224}Ra, and 43–90 dpm m^{-3} ^{226}Ra. Here salinity ranged from 11 to 33.5 and near the stream mouth we observed significant stratification of the water column with a buoyant freshwater plume with a thickness of 0.2–0.3 m. Groundwater ^{226}Ra activities across the watershed were 60–200 dpm m^{-3} (n = 8).
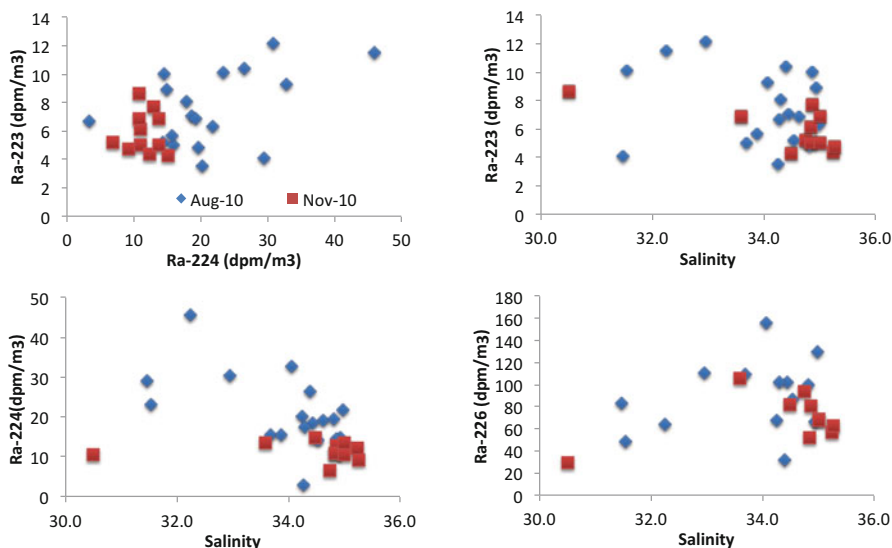

Fig. 8.2 Radium isotope distribution against salinity along transects T1–T3 in northwest Kaneohe Bay

3.2 Radon Tracer Distribution

The radon survey in northwest Kaneohe Bay in August 2010 was performed during high-and falling tides therefore it does not reflect average SGD inputs, rather a lower limit of coastal radon activities. It can be expected that highest SGD occurs along the shoreline so we focused our survey parallel to the shoreline and also made several transects in a cross-shelf direction (Fig. 8.1). Radon activities varied from 250 to 2100 dpm m^{-3} and were moderately (10x) elevated over parent-supported activities of 100–160 dpm m^{-3} estimated from dissolved ^{226}Ra measurements. In the central section of the bay activities were similar in magnitude along the coastline as well as in the Heeia fishpond.

In the fishpond the survey was performed at high tide and the measured activities were 870–2800 dpm m^{-3}. The highest activities clustered in the SW corner of the pond and near the stream mouth.

Radon time series measurement in the coastal water was performed at Coconut Island, which is in central Kaneohe Bay about 750 m from the main shoreline (Fig. 8.1). The measurements confirmed a significant tidal influence on coastal radon activities (Fig. 8.3). The observed activities ranged between 0 and 1800 dpm m^{-3}. During high tide radon levels decreased to ocean levels of ~60 dpm m^{-3} and during low tide the activities increased due to intensifying SGD and lower mixing with offshore waters. There was a period (February 1–18, 2012) of elevated baseline radon when even during periods of high tide radon activities did not decrease to supported levels of 60 dpm m^{-3}. This period showed the highest SGD fluxes during the 2-month monitoring program.

Groundwater radon concentrations were $150,000 \pm 190,000$ dpm m^{-3} in high-level groundwater (n = 8) and $90,000 \pm 80,000$ dpm m^{-3} in the wetland groundwater (n = 11).

3.3 Nutrient Distribution

Nutrient concentrations in the watershed and the coastal ocean are summarized in Table 8.1. As expected, groundwater and streams were more enriched in nutrients than coastal waters in the bay and the fishpond. Nitrate concentrations were similar in northwest Kaneohe Bay in August and November, 2010. The wetland water masses were significantly reduced in silicate and contained more reduced ammonium than nitrate. There was a large variability in DIN concentrations in the wetland. Nitrogen was mostly in the form of highly variable ammonium with an average concentration of 21 ± 140 μM; nitrate + nitrite concentrations averaged 0.3 ± 35 μM. Dissolved oxygen varied between 1 and 15 % saturation and phosphate concentrations were 0.6 ± 0.3 μM. Surface water, including the stream in the wetland, had <0.5 μM nitrate + nitrite, 11 ± 80 μM ammonium, and 0.2 ± 0.1 μM of phosphate. Dissolved oxygen concentrations were 56 ± 50 % saturation.

Table 8.1 Surface and groundwater dissolved inorganic nitrogen (DIN), dissolved inorganic phosphorus (DIP), and silicate concentrations (µM) in Kaneohe watershed in Waikane stream located in the northwest sector (Smith et al. 1981), Kaneohe Bay surface water (sw) August, Kaneohe Bay surface water November, He'eia fishpond surface water, He'eia wetland surface water, He'eia wetland groundwater (gw), and Waikane groundwater (all determined during this study)

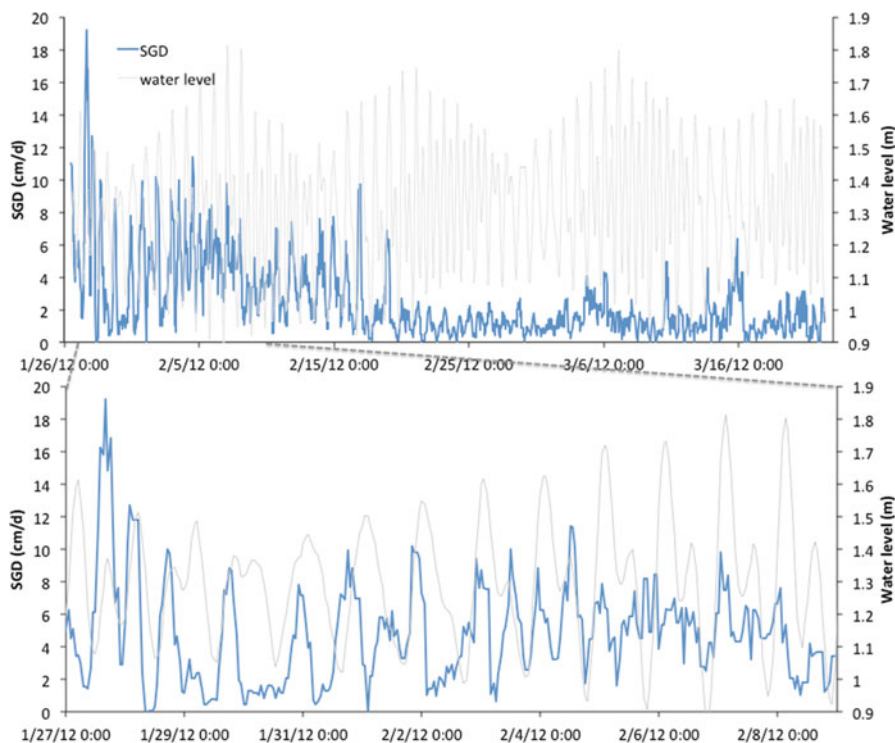|	Sampling date	Number of samples	DIN	DIP	Silicate	DIN: DIP
Waikane sw	2/6/2013	7	12 ± 3	1.6 ± 0.5	540 ± 92	8
Kaneohe sw	8/17/2010	9	0.79 ± 0.43	0.051 ± 0.033	14.8 ± 6.0	15
Kaneohe sw	11/5/2010	11	0.68 ± 0.36	0.073 ± 0.100	6.9 ± 3.7	9
He'eia FP sw	11/19/2013	9	0.64 ± 0.53	0.11 ± 0.09	65 ± 75	6
He'eia wl sw	2–5/2013	16	11 ± 5	0.22 ± 0.14	220 ± 81	50
He'eia wl gw	2–5/2013	8	21 ± 144	0.56 ± 0.25	170 ± 53	38
Waikane gw	2/6/2013	7	12 ± 3	1.6 ± 0.5	540 ± 92	8

Fig. 8.3 A 1-h resolution SGD (cm d^{-1}) derived from a coastal radon record collected at Coconut Island in Kaneohe Bay, HI. The radon monitor was located on the shore of the island about 750 m from the major coastline's groundwater sources

4   Discussion

Coastal groundwater fluxes can be estimated indirectly using a mass balance of naturally occurring radioactive isotopes (Charette et al. 2008). We employ a multi-tracer approach utilizing radium isotopes to estimate SGD (Sects. 4.1–4.3) as described in Moore (1996) and Moore (2000a) then complement these estimates with radon derived groundwater fluxes (Sects. 4.4 and 4.5) utilizing methods described in Dulaiova et al. (2010) and Burnett and Dulaiova (2003). These methods are based on the continuous regeneration of radon and radium isotopes from U- and Th-bearing minerals via radioactive decay in aquifers. Groundwater becomes enriched in these isotopes because the water-to-solids surface area ratio is small and the water layer around the solids effectively captures the recoiling newly produced radionuclides. Owing to the absence of major sources, surface waters have orders of magnitude lower activities of these isotopes. A coastal mass balance can then be formulated to calculate the amount of the tracer derived by SGD after accounting for all other sources of these isotopes.

Since one of the goals of SGD studies is to demonstrate the effect of SGD on coastal water quality, some important aspects to consider are coastal nutrient inventories (Sect. 4.6) and the SGD-derived nutrient fluxes (Sect. 4.7), the rates of their dilution by mixing, and the degree to which these inputs get taken up by biological and inorganic processes. The processes listed above depend on the rate of delivery and residence time of nutrients in the coastal water. In Sect. 4.8 we use radium isotopes to estimate the age of SGD-derived conservative solutes as a measure of coastal residence time (Moore 2000b; Moore et al. 2006). This is the amount of time it takes for the nutrients to leave the investigated water body either by along-shore currents or by mixing into the offshore ocean. In Sect. 4.9 we use these residence times in combination with terrestrial fluxes to compare coastal nutrient mass balances in different sectors in Kaneohe Bay. Finally estuarine net nutrient removal rates are derived based on marine nutrient profiles and the combined SGD and stream nutrient fluxes (Sect. 4.10).

4.1   Horizontal Mixing Rates in Northwest Kaneohe Bay

The presence of excess radium isotopes in the nearshore region is an indication of coastal radium inputs from a combination of groundwater, stream, and suspended particulate sources at a rate at which elevated radium concentrations persist despite their radioactive decay (^{224}Ra half-life is 3.7 days and ^{223}Ra is 11.4 days) and mixing losses. The short- and long-lived radium distribution and mass balance can be used to determine SGD, in which the first step is to calculate horizontal mixing rates. For the same mixing ^{223}Ra returns estimates of smaller relative uncertainties on horizontal diffusion coefficient estimates than ^{224}Ra because of its longer half-
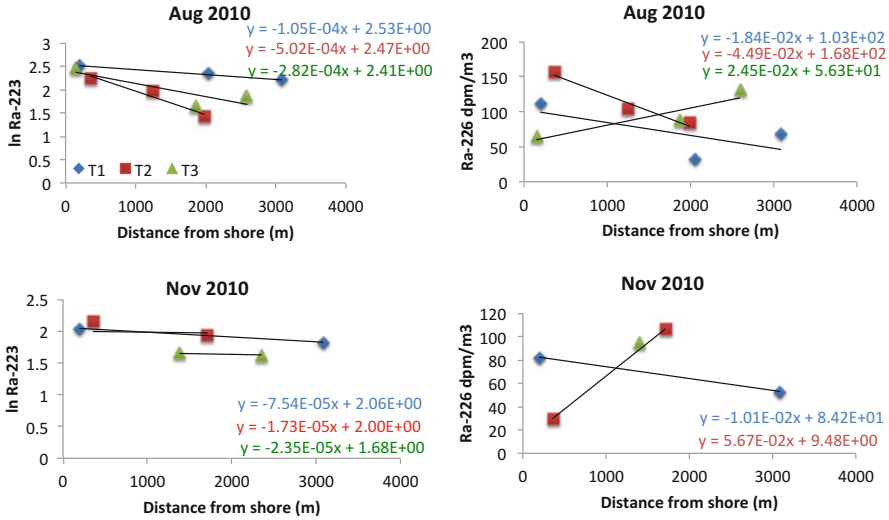
Fig. 8.4 Short and long-lived radium distribution over distance form shoreline on transects T1–T3 in the northwest sector of Kaneohe Bay in August and November, 2010

life and more gradual cross-shore gradients (Knee et al. 2011). Therefore we used [223]Ra as an independent mixing tracer for the nearshore region of Kaneohe Bay.

In a system controlled by eddy diffusion, we can use the distribution of [223]Ra to calculate a horizontal eddy diffusion coefficient (K_h, Moore 2000a) under the assumption that radium distribution depends on two processes, radioactive decay and mixing. We only had three sampling points on each transect so were not able to evaluate the influence of advection (concave or convex shape, break in slope), and we assumed that the system was controlled by eddy diffusion and that the dominant water transport was in a cross-shore direction neglecting alongshore currents. The water column was stratified along all 3 transects preventing significant radium diffusion inputs from benthic sources.

We derived gradients of the natural logarithm of [223]Ra from the three transects. If the above-stated assumptions are accurate then the ln[223]Ra slope depended only on the decay constant λ_{223} and eddy diffusion coefficient K_h (Moore 2000a):

$$slope = \sqrt{\frac{\lambda_{223}}{K_h}}. \tag{8.1}$$

The slopes for the three transects (T1, T2, T3; Fig. 8.4) were calculated individually (and averaged -2.96×10^{-4} m^{-1}) resulting in an average eddy diffusion coefficient K_h of 25 m^2 s^{-1} and 57 m^2 s^{-1} in August and November 2010, respectively. The relative uncertainty on these diffusion coefficients was 17–30 % resulting from having only 3 sampling points on each transect, R^2 of slopes >0.9 and a [223]Ra measurement error of 17–22 %.

4.2 Coastal ^{226}Ra Fluxes in Northwest Kaneohe Bay

Next, we used the eddy diffusion coefficient and the concentration gradient of ^{226}Ra along the same transects (Fig. 8.1) to estimate the coastal flux of ^{226}Ra to the ocean. Ra-226 in this case represents a conservative tracer as due to its long half-life ($T_{1/2} = 1600$ year) it does not decay on the time scale of coastal transport processes.

The linear ^{226}Ra gradients (Fig. 8.4) were -1.0×10^{-2} dpm m^{-3} m^{-1} for T1 and -1.8×10^{-2} dpm m^{-3} m^{-1} for T2 in August 2010, while T3 had a positive slope. In November 2010, we could only used data from T1, as T2 had a positive slope and T3 was incomplete with only one sampling point. The positive slopes suggested that there was either an offshore SGD source near T3, some lateral transport of high-radium water masses from upstream coastal areas, or that radium was removed in the coastal region by sorption onto suspended particles. In this case we surmise that the positive slope can be explained by radium delivered by the Waihee River (fluxes derived from USGS station indicated in Table 8.2) located just south of T3, which may preferentially flow along a coral patch to the offshore sections of T2 and T3. Alternatively, it is possible that there was some radium sorption to particles as stream particle inputs at the beginning of T3 resulted in coastal suspended sediment load of 0.017 g L^{-1} and 0.012 g L^{-1} in August and November, respectively. We observed that the suspended particles in this watershed were enriched in iron (surmised based on color and elevated dissolved iron concentration in groundwater, Dulaiova unpublished results) most probably in form of iron (oxy)hydroxide precipitates that have shown to attract radium even at elevated salinities (Gonneea et al. 2008).

On average the surface mixed layer was 1 m thick at T1 and 1.4 m thick at T2 as determined from salinity depth profiles along the transects. Individual aquifer sector coastline lengths were used to calculate the offshore ^{226}Ra fluxes of 1.6×10^{8} dpm d^{-1}(T1) and 1.3×10^{7} dpm d^{-1} (T2) in August and 1.7×10^{8} dpm d^{-1} (T1) in November. These ^{226}Ra fluxes were supported by streams, groundwater discharge and desorption from suspended particles delivered by streams. Stream water and sediment fluxes were scaled according to the coastline length of each transect (Table 8.2). River discharge and suspended particulate flux from the streams was determined using USGS stream gauges and relationships derived by Hoover et al. (2009). The estimated sediment load was 170,000 g d^{-1} in August and 61,500,000 g d^{-1} in November. We used literature values (Krest et al. 1999) to estimate radium desorption from sediments recognizing that this input may actually be much smaller due to the iron enrichment of the particles that would not release radium as easily as the sediment types studied by Krest et al. (1999), which were suspended and bottom sediments from the Mississippi delta. We estimate a suspended particle desorption flux for ^{226}Ra of 1.1×10^{5} dpm d^{-1} and 1.29×10^{7} dpm d^{-1} in August and November 2010, respectively. Inspection of all sources revealed that the total ^{226}Ra flux was clearly dominated by groundwater inputs as river and suspended particle inputs were 1–3 orders of magnitude lower than the total radium flux. Any uncertainty in these estimates therefore was insignificant in terms of the final SGD fluxes.

Table 8.2 Characteristics of the study domains in the northwest sector of Kaneohe Bay (NB), central Kaneohe Bay (CB) not including He'eia fishpond, and the He'eia fishpond (HFP)

		Coastl. length	Stream	SGD-Rn		SGD-Ra-223/6		SGD-Ra-226		Mixing coefficient	Residence time	
											Mixing	Ra age
		m	$m^3\,d^{-1}$	$m^3\,d^{-1}$	$m^3\,m^{-1}\,d^{-1}$	$m^3\,d^{-1}$	$m^3\,m^{-1}\,d^{-1}$	$m^3\,d^{-1}$	$m^3\,m^{-1}\,d^{-1}$	$m^2\,d^{-1}$	d	d
NB Aug-10	T1	1530	1.9E+4	5.5E+4	36	6.0E+5	393	1.7E+4	11	5.5E+6	0.9	3.4–6.6
	T2	840	3.0E+4	2.3E+4	27	3.3E+4	40	1.1E+5	133	2.4E+5	8	0–3.2
	T3	2800	1.8E+4	2.9E+4	10			4.2E+5	150	7.6E+5	4	0.1–2.8
NB total Aug		5170	6.8E+4	1.1E+5	20	1.1E+6	217	5.1E+5	98		8	6.6
NB Nov-10	T1	1530	1.7E+5			6.3E+5	413	2.2E+5	141	1.1E+7	0.4	0.9–1.3
	T2	840	2.6E+5					–		2.0E+8	0.01	0.1–3.6
	T3	2800	1.6E+5					–		1.1E+8	0.03	0–3.2
NB total Nov		5170	6.0E+5			2.1E+6	413	7.3E+5	141		0.4	3.6
CB Aug-10		7700	1.0E+4	4.6E+4	6			2.1E+5	27			0–10
HFP Nov-13		1250	2.1E+3	2.5E+3	2							2–6

Transects T1–T3 are shown in Fig. 8.1. Coastline length and stream discharge are based on USGS stream gauges in the watershed, SGD fluxes (Sects. 4.1–4.5) and residence times are derived from the diffusion coefficients and apparent radium ages (Sect. 4.8), and are indicated for the individual parts of the sectors, including two different time-periods for NB. For comparison, the volume of water exchanged between average low and high tides is $10 \times 10^6\ m^3$ in NB and $18 \times 10^6\ m^3$ in CB (Bathen 1986)

4.3   Submarine Groundwater Discharge in Northwest and Central Kaneohe Bay Estimated via Radium Approaches

SGD-derived radium fluxes were calculated by subtracting stream and particle desorption Ra fluxes from total ^{226}Ra fluxes. The net groundwater derived flux was then divided by groundwater ^{226}Ra concentrations of 200 dpm m^{-3}. The individual SGD estimates (Table 8.2) had ~36 % relative uncertainty, which was calculated via error propagation of the individual terms: diffusion coefficients 30 %, Ra flux 35 %, groundwater Ra activity 10 %.

We normalized SGD estimates from T1 and T2 as discharge per meter shoreline and extrapolated SGD to the whole northwestern bay. SGD was 20 times higher than stream inputs in August and 3 times higher in November, 2010 (Fig. 8.5). We observed a change in the SGD:stream discharge ratio, which was expected as during
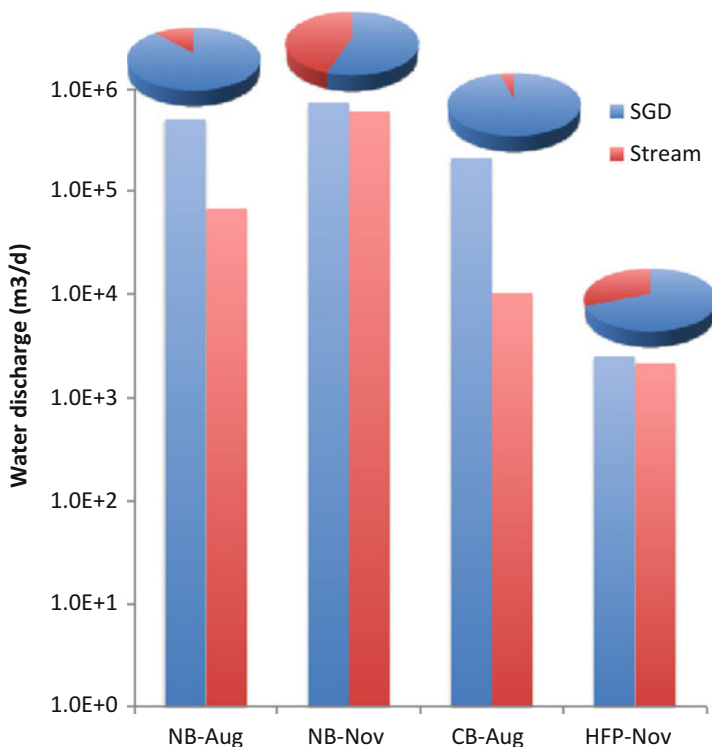

Fig. 8.5 The bars represent the magnitude of SGD (*blue*) and stream (*red*) discharge (m^3/d) for northwestern Kaneohe Bay in August (NB-Aug) and November (NB-Nov), central bay in August (CB-Aug), and Heeia fishpond in November (HFP-Nov). The y-axis is a logarithmic scale for better comparison between NB and HFP locations. The pie charts indicate relative DIN contribution of SGD and streams to the bay

the dry season in August groundwater flux was the major terrestrial water source to the coastline and the streams were only fed by baseflow. The November sampling was performed following the first big storm after the dry season, which resulted in increased streamflow. The groundwater aquifer responded much more slowly to the increased recharge and we did not observe an immediate increase in SGD. In fact we have shown that SGD had a 2–3 month lag in responding to increase in recharge in the Kaneohe Watershed (Leta et al. 2015).

We also used another approach to calculate SGD that involved a ^{226}Ra mass-balance and residence times (Moore 1996). Coastal activities of ^{226}Ra were multiplied by the volume of the water mass and divided by the coastal residence time derived in Sect. 4.6. In this way a replacement rate of radium was estimated which, at a steady-state, should be equal to ^{226}Ra inputs via streams and SGD. Stream and particle sources were subtracted from the total radium fluxes and finally the SGD-derived radium flux was divided by groundwater ^{226}Ra activity. The resulting SGD was 2–4 times lower than the estimates described above (Table 8.2) but still dominated over stream water discharge.

A point to keep in mind is that SGD is a mixture of brackish groundwater and recirculated seawater, and as a consequence cannot be compared in terms of freshwater fluxes to stream inputs. The salty fraction of SGD has been shown to represent 40–80 % of total fluxes in Hawaii (Street et al. 2008; Kleven 2014; Glenn et al. 2013; Mayfield 2013), seawater recirculation through the coastal aquifer therefore contributes significantly to total SGD. Yet brackish and salty SGD play an equal role as nutrient pathways and as we show below, nutrient fluxes via total SGD must be considered in nutrient coastal mass balances.

4.4 Submarine Groundwater Discharge in Northwest and Central Kaneohe Bay Estimated Using a Radon and Radium Mass Balance

A coastal radon survey was performed to determine surface water radon inventories in August 2010 (Fig. 8.1). The measured concentrations were used to calculate SGD fluxes based on the following equation:

$$Q_{SGD} = \frac{A_{Rn\_cw}*V}{\tau*A_{Rn\_gw}}, \tag{8.2}$$

where Q_{SGD} is total submarine groundwater discharge (m^3 d^{-1}), A_{Rn_cw} are coastal water radon activities corrected for non-SGD sources (diffusion from sediments, in situ radioactive production from ^{226}Ra, offshore inputs) and losses (evasion to the atmosphere, radioactive decay), A_{Rn_gw} is groundwater radon activity (dpm m^{-3}), V is the volume of the coastal water box that the measurement represents (m^3) and τ is the flushing rate of the coastal zone, which in this case was a tidal cycle (Dulaiova et al. 2010).

SGD determined by the radon survey amounted to $1.1 \times 10^5 \, \mathrm{m}^3 \, \mathrm{d}^{-1}$ or $20 \, \mathrm{m}^3 \, \mathrm{m}^{-1} \, \mathrm{d}^{-1}$ in the northwestern sector and $4.6 \times 10^4 \, \mathrm{m}^3 \, \mathrm{d}^{-1}$ or $6 \, \mathrm{m}^3 \, \mathrm{m}^{-1} \, \mathrm{d}^{-1}$ in central Kaneohe. We expect that SGD would be associated with lower salinity of bay water. The lowest salinities observed during the survey were at T2 (17–29) and the average salinity in the northwestern part of the bay was 32.1, the minimum in central Kaneohe Bay was 31.3 and the average 34.7.

We applied the ^{226}Ra mass balance (Moore 1996, 2003) in the central sector of the bay and calculated $2.1 \times 10^5 \, \mathrm{m}^3 \, \mathrm{d}^{-1}$ or $27 \, \mathrm{m}^3 \, \mathrm{m}^{-1} \, \mathrm{d}^{-1}$ of SGD. In all sectors SGD fluxes calculated via radon were 2–10 times lower than the radium mass balance derived fluxes.

At a later date in January–March 2012, post-dating the transect work, a time-series radon-monitoring station was installed southeast of T3 at Coconut Island. This station likely only captured SGD emanating locally from the 117,000 m² area of the small island's freshwater lens. The record revealed tidal as well as longer-term patterns of change in the radon signature reflecting changes in groundwater discharge and coastal conditions (SGD, rain, wind, mixing). The estimated groundwater advection rates, derived by using methods described by Burnett and Dulaiova (2003), ranged from 0 at high tide to a maximum of 19 cm d^{-1}, which occurred in the earlier part of the deployment in January 2012 (Fig. 8.3). These advection rates were relatively low compared to other observed rates around the island and reflect only a localized SGD from the island's small aquifer. The records showed that SGD had a tidal signature with higher fluxes at low and rising tides and lower advection rates at high tide. There are two reasons for this observed pattern: (1) at high tide the hydraulic gradient between the ocean and the coastal aquifer is smaller or even reversed relative to low tide, resulting in a smaller driving force hence less SGD; and/or (2) during flood tide the coastal SGD chemical signature is diluted because groundwater is discharged into a larger water mass. Over the time-scale of the deployment, the record showed higher SGD in January and the first half of February with a decrease of baseline fluxes in the second half of February and throughout March.

The inset on Fig. 8.3 shows a selected time interval during which neap tide switched to spring tide and the SGD dynamics mimicked the tidal progression, showing diurnal and semi-diurnal patterns. Because tides were not the only driving force behind the hydraulic gradient (precipitation, hydraulic conductivity, groundwater withdrawals and other forcing factors), we did not observe a corresponding pattern between the magnitude of SGD and tidal range.

The fact that SGD dynamics is so strongly influenced by tides has implications for the radon survey as it was performed in the tidally influenced nearshore region and only reflected a snap-shot SGD at the time of measurement. Since the northwest Kaneohe Bay survey was done at high tide, when SGD was at its lowest point, it represents a below-average estimate of SGD. The radium techniques employed here on the other hand integrated SGD over the time period of the water residence time along the sampled transects and better represented the overall groundwater fluxes. We therefore conclude that the twofold to tenfold difference in SGD estimates via radon and radium isotopes in northwest Kaneohe Bay was due to the different spatial and temporal sensitivity of these approaches. Both methods revealed large spatial heterogeneity in SGD (Fig. 8.1 and Table 8.2).

4.5 SGD into Heeia Fishpond: Central Kaneohe Bay via a Combined Radon and Radon Mass Balance

Measured radon inventories and radium isotope-derived water ages (see below) were applied in Heeia fishpond to derive SGD using Eq. (8.2). We corrected the measured radon inventories for atmospheric evasion losses and radioactive decay. The groundwater radon activities applied here were derived from the wetland located directly upstream of the fishpond. The resulting SGD flux was 2500 m^3 d^{-1}, which was about equal to the estimated contribution of stream discharge into the fishpond (2200 m^3 d^{-1} derived from a USGS stream gauge at Haiku, Fig. 8.5). A salinity mass balance calculated for the pond was also calculated which suggested that 88 % of SGD was brackish water contributed by recirculated seawater (Kleven 2014). There was elevated SGD along the seawall in the pond suggesting either a presence of a breached impermeable layer forcing groundwater to discharge offshore or that porewaters were pushed out of the sediments by tidally driven hydraulic gradient set up across the sea wall. This portion of the SGD, even though was not identified as fresh water discharge, may be a significant contributor of nutrients because porewaters in the bottom sediments in the fishpond are enriched in nitrogen and silicates (Briggs et al. 2013).

4.6 Watershed Nutrient Concentrations

Nutrient concentrations in groundwater within the individual sub-watersheds of Kaneohe Bay varied with land-cover between the watersheds. We collected samples from the high level aquifer in the upper watershed (n = 8) where the nutrient concentrations were uniform with little variation: 12.1 ± 2.9 µM of nitrate + nitrite, 1.6 ± 0.5 µM of inorganic phosphate and 545 ± 96 µM of silicate (Table 8.1). Oxygen concentrations were >90 % saturation and organic nutrient species were a negligible part of totals. Due to the porous, highly conductive nature of the basalt there is a direct surface water groundwater interaction and, except after significant storm events, baseflow is a major contributor to streamflow and nutrients (Izuka et al. 1994). As a consequence of this connection, stream nutrient concentrations equaled groundwater concentrations. Hoover (2002) derived discharge vs. nutrient concentration relationships and concluded that at baseflow the streams had the same silicate, nitrate and phosphate concentrations as groundwater—on average 400–500 µM silicate, 5–10 µM nitrate + nitrite, and 0.5–1.2 µM of phosphate. Surface runoff only diluted silicate concentrations but nitrate and phosphate concentrations did not change significantly after storm events (Hoover et al. 2009).

The conservative nutrient behavior in all of Kaneohe watershed assumed by Hoover et al. (2009) contrasted greatly with our observations in the Heeia watershed where the stream and groundwater flowpaths are intercepted by a coastal wetland before draining into central Kaneohe Bay. Silicate concentration in the

stream and groundwater were only 170 ± 50 μM and 220 ± 80 μM, respectively. The lower silicate concentration in groundwater is likely due to its uptake by wetland grasses and macrophytes that are abundant in the wetland, and which are known to draw down silicate (Schoelynck et al. 2010). Although our study did not specifically target wetland nutrient uptake mechanisms, there was no obvious variation in wetland nutrient concentrations with stream discharge.

4.7   Nutrient Fluxes

Stream-derived nutrient fluxes into northwest Kaneohe Bay were calculated by multiplying baseflow and groundwater nutrient concentrations by stream discharge determined from USGS stream gauges and methods described by Hoover (2002). In the central bay, Heeia stream discharge was multiplied by the measured stream and wetland surface water nutrient concentrations.

Groundwater derived nutrient fluxes were calculated by multiplying SGD (derived using the radium-transect method) and well groundwater nutrient concentrations for northwest Kaneohe Bay ($m^3/d \times mol/m^3 = mol/d$), and SGD multiplied by wetland groundwater nutrient concentrations in central Kaneohe Bay (Table 8.3). This approach assumes that nutrients do not undergo any biogeochemical removal along the groundwater flowpath between the sampled location and their discharge at the coastline.

Our data indicate that brackish pore water nutrient values for the fishpond were in the same range as wetland fresh groundwater nutrient concentrations (Briggs et al. 2013; Kleven 2014). Also, Smith et al. (1981) reported nutrient concentrations in northwest and central Kaneohe Bay in porewater in the upper 0.3 m of lagoon sediments that were comparable to well groundwater concentrations, 80 ± 27 and 145 ± 60 of DIN and 16 ± 4 and 9 ± 5 of phosphate for northwest and central bay, respectively. This suggests that recirculated seawater has similar nutrient levels as fresh groundwater. This observation is in contrast to, for example, observations on the Kona coast of the Hawaii Island where linear mixing relationship was found between nutrients and salinity in coastal aquifers implying that recirculated seawater diluted groundwater nutrient concentrations (Paytan et al. 2006). As our groundwater and porewater nutrient comparison shows, dilution of groundwater nutrients by recirculated seawater does not seem to occur in Kaneohe Bay, where recirculated seawater flows through organic rich alluvial sediments rather than young basalt, and is equally enriched in nutrients. Nevertheless we acknowledge that biogeochemical transformations may remove nitrogen and phosphorus from porewaters along the groundwater recirculation path and our nutrient flux estimates may be higher than actual fluxes. Also, unlike stream discharge and fresh SGD, recirculated seawater does not contribute new nutrients to the bay, it only recycles autochthonous nutrients released by remineralization of buried organic matter.

The derived DIN fluxes were 5–10 times higher via SGD than surface runoff in all regions (Fig. 8.5), proving SGD to be a significant contributor to coastal nitrogen

Table 8.3 Nutrient fluxes by stream surface inputs and total SGD derived from SGD fluxes indicated in Table 8.2 and nutrient end-member concentrations listed in Table 8.1

Nutrient fluxes (mol d^{-1})

		Stream			SGD Rn-derived			SGD Ra-223/6-derived			SGD Ra-226-derived		
		DIN	DIP	Silicate	DIN	DIP	Silicate	DIN	DIP	Silicate	DIN	DIP	Silicate
NB	Aug-10	229	31	10,310	656	87	29,509	7221	963	324,961	207	28	9309
		360	48	16,202	271	36	12,211	401	54	18,064	1342	179	60,404
		221	29	9942	344	46	15,487				5026	670	226,165
NB total Aug		810	108	36,453	1271	170	57,207	13,436	1791	604,624	6080	811	273,608
NB	Nov-10	2018	269	58,858				7576	1010	340,913	2595	346	116,753
		3171	423	92,492									
		1946	259	56,756									
NB total Nov		7135	951	208,106				25,599	3413	1,151,974	8767	1169	394,520
CB Aug-10		115	2	2291	502	10	16,190				2522	336	113,494
HFP Nov-13		24	0.5	471	53	1	425						

budgets. Phosphate fluxes were lower via SGD than surface runoff which can be explained by the coupling between iron and phosphorus chemistry and phosphate occlusion in iron and aluminum (hydr)oxides in the aquifer (e.g. Spiteri et al. 2008). Silicate fluxes via SGD and surface runoff were comparable in northwest Kaneohe Bay, and were dominated by surface runoff in the central bay and in the fishpond (Table 8.2). This is expected as we see a significant silicate uptake in wetland groundwater samples, therefore SGD-derived silicate is lower than stream discharge that is fed partially by baseflow and surface runoff. Silicate fluxes in terms of SGD and surface runoff ratios were comparable to findings in the same (Hoover et al. 2009) and similar watersheds in other studies (e.g. Garrison et al. 2003; Mayfield 2013).

4.8 Coastal Residence Times

Coastal inventories of conservative solutes depend on the magnitude of their terrestrial inputs (SGD, stream, benthic fluxes) as well as on coastal mixing and dilution driven by oceanic processes. The higher the terrestrial fluxes the higher the coastal inventory and, the more effective the mixing with offshore water the less likely it is that a pollutant will have an impact on the coastal ecosystem.

The Ra-derived horizontal diffusion coefficients provide a measure of lateral mixing and can also be used to quantify residence times. In our setting, a residence time estimate is also analogous to a flushing rate (flow rate/volume). Windom et al. (2006) have shown that coastal residence time of geochemical components approximated by Ra can be related to the mixing coefficient using the following relationship:

$$t = \frac{L^2}{2K_h} \tag{8.3}$$

where t is residence time (days), K_h is the mixing coefficient ($m^2 d^{-1}$) and L is the length of the transect over which the mixing coefficient was estimated (m). In northwest bay, application of this method resulted in residence times of 0.9–8 days in August and 0.01–0.4 days in November, 2010. Indeed, in August the observed radium inventories were higher than in November (Fig. 8.2). Radium isotope ratios have also been used as a measure of coastal residence time by determining so called apparent radium ages (Moore 2000b; Kelly and Moran 2002). In this approach a short-lived isotope is normalized to a long-lived isotope of radium and because of their chemically identical behavior only their radioactive decay drives changes in their activity ratio once the water mass is isolated from their parent nuclides. This method requires that there is a uniform activity ratio in all contributing radium sources (SGD, streams, diffusion) and this assumption does not seem to hold true in Kaneohe Bay. Measurements in Heeia stream resulted in $^{224}Ra/^{223}Ra$ activity ratio of 1.1 similar to observations in other locations on Oahu (Wailupe by Holleman 2011;

Waimanalo, Dulaiova, unpublished results). The activity ratio for these same isotopes was closer to 7 in brackish SGD and to 4 in fresh SGD (Kleven 2014). A higher activity ratio is a result of faster regeneration rate of ^{224}Ra, and hence its higher enrichment in comparison to ^{223}Ra in groundwaters of short residence time (such as recirculated seawater) in which radioactive equilibrium has not been established. Since at any time, coastal water is a mixture of stream inputs, fresh SGD, and brackish SGD, it was only possible to relate apparent radium ages of offshore water masses to the composite coastal isotope signature rather than the individual groundwater and stream activity ratios. The composite coastal activity ratio was ~4 in August when coastal radium inventories were driven by SGD inputs and ~2 in November when stream discharge also contributed significantly to coastal radium inventories. Apparent radium ages were then estimated using the following equation (Moore 2000b):

$$t \;=\; \ln \frac{^{224}Ra_i/^{223}Ra_i}{^{224}Ra_o/^{223}Ra_o} * \frac{1}{\lambda_{224} - \lambda_{223}}. \tag{8.4}$$

These ages are based on the faster decay of the short-lived ^{224}Ra (λ_{224} is its decay constant in days^{-1}) in comparison to ^{223}Ra (λ_{223} decay constant of ^{223}Ra) in an offshore water mass (Ra$_o$) assuming a composite nearshore end-member (Ra$_i$) and that both isotopes are subjected to the same dilution by mixing. The resulting average apparent radium ages were 2.7 days and 1.4 days in August and November, respectively. The uncertainty on these ages was estimated to be 50–100 % according to evaluations described by Knee et al. (2011) because the activity ratio method is not very sensitive for water ages below ~3.5 days. Both methods suggested a faster mixing rate in November than in August 2010 (Table 8.2). Lowe et al. (2009) used a coupled wave circulation numerical model and showed that wave forcing is the dominant mechanism driving currents and flushing in Kaneohe Bay. According to their result, for the conditions observed on August 16, 2010 (wave height 1–2 m and wave direction 90°; obtained for Mokapu Buoy at http://cdip.ucsd.edu) and November 4, 2010 (2–3 m and 360°) the residence times were 1.3 and 0.8 days, respectively.

Apparent water ages in the Heeia Fishpond varied from <2 days in the section that was well flushed by the incoming stream, to about 6 days in the SW corner of the pond that has a restricted circulation (Kleven 2014).

4.9 Coastal Nutrient Budgets

Terrestrial nutrient contributions to coastal inventories were calculated as the sum of stream and SGD inputs. To estimate coastal inventories we used the measured coastal nutrient concentrations and estimated water volumes of the lower salinity water layer along our radium and radon survey transects in northwest and central

Table 8.4 Coastal parameters with terrestrial and recycled nutrient inputs from streams and SGD, conservative geochemical residence time (T_{Ra}), DIN residence time with respect to coastal inventory and stream + SGD fluxes (T_N), volume of the coastal domain (V), and DIN inventory N (mol)

	Input fluxes	Coastal parameters
	NB_Aug	
SGD (m^3 d^{-1})	100,000(Rn)–1,400,000(Ra)	T_{Ra}: 6.6–8 & T_N: 0.5–4.5 d
SGD DIN (mol d^{-1})	1330–17,400	V: $13 \times 10e6$ m^3
Stream (m^3 d^{-1})	68,000	N: 10,200 mol
Stream DIN (mol d^{-1})	810	
	NB_Nov	
	2,000,000(Ra)	T_{Ra}: 0.4–3.6 & T_N: 0.3 d
	24,000	V: $13x10e6$ m^3
	600,000	N: 8800 mol
	7100	
	CB_Aug	
	91,000(Rn)	T_{Ra}: 10 & T_N: 12.4 d
	1000	V: $19 \times 10e6$ m^3
	10,000	N: 13,800 mol
	110	
	HFP_Nov	
	2500(Rn)	T_{Ra}: 2–6 & T_N: 2.3 d
	53	V: $28 \times 10e4$ m^3
	2100	N: 179 mol
	24	

NB is northwest sector of Kaneohe bay, *CB* is the central sector, and *HFP* is He'eia fishpond

Kaneohe Bay, and for the fishpond the volume of the whole pond was considered. For the transects, this approach encompassed most of the northwest and central bay area affected by SGD and stream inputs. Table 8.4 illustrates terrestrial nitrogen fluxes, coastal inventories, and conservative coastal residence times for each investigated sector in Kaneohe Bay: northwest and central Kaneohe Bay, and Heeia Fishpond. The radium diffusion coefficient-derived SGD DIN fluxes were an order of magnitude higher than stream inputs, suggesting that SGD was an overwhelming source of DIN to the bay. The radon mass-balance approach resulted in DIN fluxes more comparable to stream fluxes and the [226]Ra mass balance-derived fluxes fall in between the two estimates.

Because of its volume being the largest, central Kaneohe Bay represented the highest inventory of nitrogen, although coastal DIN concentrations were comparable across all three sectors (Table 8.1). DIN fluxes in all sectors were dominated by groundwater inputs. Calculated SGD fluxes were highest in northwest Kaneohe Bay regardless of the method used, contributing as much as 10^5–10^6 m^3 d^{-1} of brackish and recirculated seawater discharge and adding 10^3–10^4 mol d^{-1} of DIN. This result is consistent with reported water budgets (Shade and Nichols 1996) in which

the northwestern sector receives 60 % of the total surface and groundwater runoff in Kaneohe Bay. Because we evaluated SGD in two contrasting periods (dry and after the first large storm) we can compare SGD and stream discharge responses. While stream inputs increased tenfold between August and November, SGD barely doubled for the same time period and we surmise that the reason for this difference was the delay in water recharge into the aquifer. Nevertheless, SGD stayed the dominant DIN source also in November.

DIN fluxes were significantly lower in the central sector, with SGD contributing 10^3 and streams 100 mol d^{-1}. In Heeia Fishpond DIN fluxes amounted to 80 mol d^{-1} in a 1:2 ratio of stream and SGD contribution.

We calculated coastal DIN residence times with respect to terrestrial inputs by dividing coastal inventories by the sum of stream and SGD fluxes. DIN residence times were lower than those derived by radium isotopes suggesting a nitrogen removal by biological uptake or abiotic processes (Drupp et al. 2011). The northwest section of Kaneohe Bay had DIN residence times <1 day and geochemical Ra-derived residence time of 3–8 days. In the central bay both estimates are ~10 days. In the fishpond DIN residence time is about 3 times less than Ra-derived estimates, again, suggesting DIN removal from the water column.

The northwest bay had shorter residence times in November, which could at least theoretically be related to nutrient uptake in the bay. Lucas et al. (2009) suggested that after nutrient limitation, estuarine retention or transit time is the major factor determining nutrient uptake. From our nutrient distribution, it was impossible to quantify any differences in DIN uptake between November and August when residence times were <1 day vs. 6–8 days, respectively (Table 8.2).

The dominance of SGD over terrestrial surface water inputs is typical for Hawaii coastlines. According to Zekster (2000) SGD from large islands is disproportionally greater than from most continental areas and represents at least 50 % of all SGD in the Pacific Ocean (Zektser 2000). This result is a consequence of high rainfall, steep topography, and permeable fractured rocks with large hydraulic conductivity that are typical for many islands. The global fresh SGD flux is estimated to be only <10 % of river discharge (Taniguchi et al. 2002). Early watershed budget estimates for Kaneohe bay for annual average stream and groundwater flow were 240 and 22×10^3 m^3 d^{-1} in 1978–1979, matching closely the global SGD to river discharge ratio of 1:10 (Smith et al. 1981). Follow-up studies of the Kaneohe watershed showed that recharge to groundwater aquifers is actually 1.5 times the volume of surface runoff (Shade and Nichols 1996) suggesting that fresh SGD may potentially be 1.5 times (less contribution to baseflow) the stream runoff. None of the water balance techniques are able to account for recirculated seawater and the discharge of brackish groundwater, however. The most often applied methods for total (fresh and saline) SGD measurements are geochemical approaches. These have been applied on local (Moore 2000a, b), regional (Windom et al. 2006), and ocean basin scales (Moore et al. 2008). For example, using the ^{228}Ra isotope mass balance Moore et al. (2008) estimated that total SGD represents 80–160 % of river discharge in the Atlantic Ocean. Another study showed that in the Atlantic and Indo-Pacific oceans, total SGD is 3 to 4 times greater than riverine freshwater fluxes

(Kwon et al. 2015). Our findings are in agreement with these results with SGD:
stream ratios ranging between 1.2 and 4, with one outlier as high as 16. These
findings demonstrate the importance of SGD for coastal geochemical budgets and
nutrient contribution to the oligothrophic Pacific Ocean surrounding the Hawaiian
Islands.

4.10 Coastal Nutrient Uptake Rates

The effects of SGD-derived nutrients on coastal water quality and ecosystems
manifest themselves to various degrees across the islands. Several studies show
that dilution and fast exchange with offshore waters results in conservative mixing
trends of DIN, DIP, and silicate without any coastal biological uptake (Dollar and
Atkinson 1992; Johnson et al. 2008). Other studies document nutrient utilization by
nearshore phytoplankton in coastal groundwater plumes (Johnson and Wiegner
2014), nitrogen uptake by algal species identified from their δ^{15}N and C:N ratios
(Dailer et al. 2010), and in some cases algal blooms dominated by invasive species
were attributed to excess nutrient loads from SGD (Smith et al. 2001). In Kaneohe
Bay the majority of studies focus on streams as the major sources of nutrients to the
bay along with sewer outfalls, which were eliminated in 1978. The significance of
stream inputs in driving nutrient and sediment concentrations and consequent
phytoplankton response has been documented in several studies (e.g. Drupp
et al. 2011; Ringuet and Mackenzie 2005; Hoover 2002, Young 2011). While
these studies focused on stream fluxes the authors noted that groundwater fluxes
were likely contributing to the observed nutrient pulses.

Our surface water dataset only covered salinities between 17 and 35.2 in the bay
and 11 and 33.4 in the fishpond. Within this narrow salinity range silicate seemed to
be the most conservative, plotting along a conservative mixing line in the pond with
a 0 salinity intercept of 348 μM (Fig. 8.6). This value fell between upland ground-
water and stream water, reflecting a mixture of water sources to the pond and
confirming our findings of silicate uptake within the watershed, as high-level
aquifers had 540 μM of silicate. In the bay the data were more scattered, but most
of the silicate concentrations were bracketed within mixing lines fitted between
stream and upland groundwater on the terrestrial side and published values of ocean
concentrations (Laws 1980). The August and November data showed similar
patterns except for the presence of lower salinity samples in November. DIP and
DIN concentrations displayed a large degree of scatter and most samples plotted
below the defined mixing lines (Fig. 8.6). If we accept our identified stream and
groundwater sources as the end-members for these samples then there must be
significant nutrient removal in the bay. There are at least three kinds of removal
processes that could be important in this environment: (1) a biological filter—
including any biological nutrient uptake; (2) a physical filter—sorption on iron-rich
particulates and clays which are especially effective in capturing P species; (3) tidal
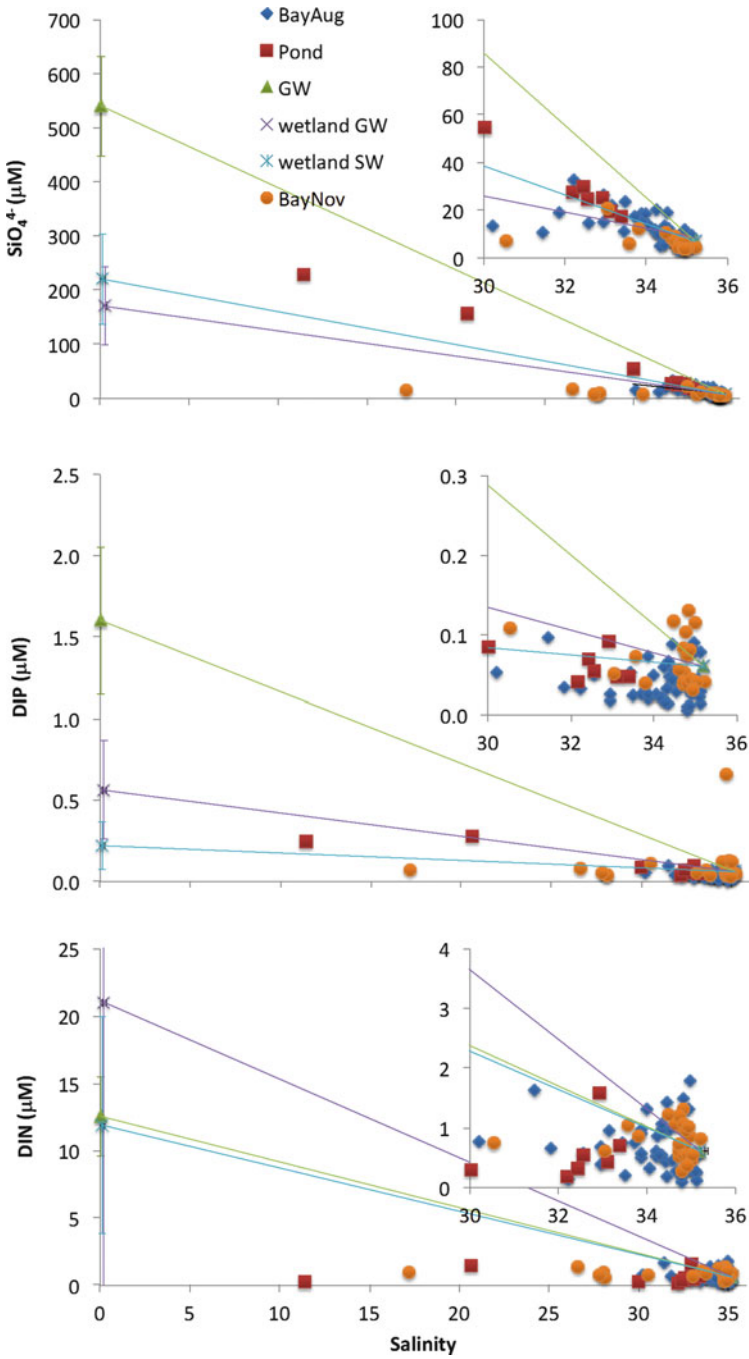exchange that significantly influence coastal nutrient concentrations via dilution

Fig. 8.6 Nutrient distribution in Kanehoe Bay in August and November 2010 and in the Heeia fishpond in November 2013. Terrestrial end-members are Waikane groundwater (GW), Heeia wetland groundwater, and Heeia wetland surface water as indicated in Table 8.1. Oceanic end-members are literature values from Laws (1980)

Table 8.5 Nutrient removal rates (R_{S+SGD}) derived from the combined inputs of stream and SGD fluxes (Q_{S+SGD}) and effective end-member intercepts (I) derived from Fig. 8.5

		I	Stream + SGD (m³ d⁻¹)			C_{R+SGD}	Estuarine removal rate (mol d⁻¹)		
		μM	$Q_{S+SGDRn}$	$Q_{S+SGDRa223/6}$	$Q_{S+SGDRa226}$	μM	$R_{S+SGDRn}$	$R_{S+SGDRa223/6}$	$R_{S+SGDRa226}$
DIN	NB_Aug	2.7	174,127	1,187,863	574,869	12	−1612	−11,000	−5323
	NB_Nov	1.2		2,733,881	1,331,188	12		−29,553	−14,390
	HFP	0.6	4639			16	−71		
DIP	NB_Aug	0.09	174,127	1,187,863	574,869	1.6	−264	−1798	−870
	NB_Nov	0.01		2,733,881	1,331,188	1.6		−4341	−2114
	HFP	0.4	4639			0.2	1		
Silicate	NB_Aug	127	174,127	1,187,863	574,869	540	−71,914	−490,588	−237,421
	NB_Nov	24.9		2,733,881	1,331,188	540		−1,408,222	−685,695
	HFP	348	4639			195	710		

The actual end-member concentration (C_{R+SGD}) was derived as the average of stream and groundwater end-members. Nutrient removal rates were calculated using Eq. (8.5); negative values indicate removal and positive values are additions of nutrients. *NB* is northwest sector of Kaneohe bay, *HFP* is He'eia Fishpond

and mixing. The rate of bulk nutrient removal encompassing all of these processes can be estimated using the effective terrestrial end-members based on the intercepts of the individual nutrient distributions. To make this estimate we use the following relationship (Maeda and Windom 1982):

$$R = IQ_T - C_T Q_T \tag{8.5}$$

where R is the nutrient removal rate in the coastal zone, I is the effective terrestrial end-member derived as the y-axis intercept of the measured bay and pond nutrient concentrations, Q_T is terrestrial water flux (stream + SGD), and C_T is the terrestrial nutrient concentration. Silicate removal rates were 73–500 mol d^{-1} and 690–1400 mol d^{-1} in August and November, respectively in the northwestern sector of the bay. There were similar significant removal rates for DIP and DIN in both time periods (Table 8.5). We did not collect enough bay nutrient data to derive nutrient removal rates for the rest of central bay.

In Heeia fishpond, DIN removal rate was 0.71 mol d^{-1} but calculated values for silicate and DIP suggest addition rather than removal (Table 8.5). In case of DIP this addition can be explained by phosphate release from suspended particles as they encounter saline waters of the pond, or benthic flux by diffusion from sediments into the shallow pond water column (Briggs et al. 2013). Silicates may be added to the water via the remineralization of the silicate rich organic matter in the wetland, contribution of high-level groundwater into SGD, or benthic flux by diffusion from sediment within the pond. Potentially, there could be remineralization and recycling of silicate within the pond water column, as well.

Our analysis shows that 78–95 % of silicate, 98 % of DIP and 83–90 % of DIN delivered to the bay and 96 % of DIN delivered to the pond is removed via biotic and/or inorganic processes. Due to the large nutrient contribution from SGD these removal rates are orders of magnitude higher than previous estimates (Smith et al. 1981).

5   Conclusions

We compared stream and submarine groundwater discharge in the northwestern and central sectors of Kaneohe bay, as well as in Heeia Fishpond. Our analysis showed that SGD in form of total (fresh+brackish) groundwater discharge was 2–4 times larger than surface inputs. We found large differences in SGD derived using different techniques for the same area. This inconsistency can be partially explained by the different time scales that the tracer techniques represent. Corresponding DIN and silicate fluxes were dominated by SGD, DIP on the other hand was delivered mostly via streams. While we observed nutrient uptake in coastal waters, nutrients were also relatively quickly removed by mixing resulting in fast coastal flushing rates.

Our study provides several major insights:

- Even our lower estimates of SGD indicate that this process must be considered in a coastal nutrient balance as groundwater delivers significant quantities of terrestrial new—as well as a recycled nutrients
- Coastal nutrient inventories are determined by the combination of SGD and coastal flushing rates. The two processes work together to influence inventory buildup and mixing offshore. Residence times vary significantly spatially and temporally in the bay.
- Seventy-eight to ninety-nine percent of nutrients delivered to the coastline are removed by biotic and abiotic processes in inner Kaneohe Bay.

References

Andersen MS, Baron L, Gudbjerg J, Gregersen J, Chapellier D, Jakobsen R, Postma D (2007) Discharge of nitrate-containing groundwater into a coastal marine environment. J Hydrol 336:98–114

Bathen KH (1968) A descriptive study of the physical oceanography of Kaneohe Bay, Oahu, Hawaii. University of Hawaii, Hawaii Institute of Marine Biology Technical Report No. 14, p 353

Beck AJ, Cochran JK, Sañudo-Wilhelmy SA (2009) Temporal trends of dissolved trace metals in Jamaica Bay, NY: importance of wastewater input and submarine groundwater discharge. Estuar Coasts 32:535–550

Beck AJ, Charette MA, Cochran JK, Gonneea ME, Peucker-Ehrenbrink B (2013) Dissolved strontium in the subterranean estuary—implications for the marine strontium isotope budget. Geochim Cosmochim Acta 117:33–52

Bokuniewicz H, Buddemeier R, Maxwell B, Smith C (2003) The typological approach to submarine ground-water discharge (SGD). Biogeochemistry 66:145–158

Bowen JL, Valiela I (2001) The ecological effects of urbanization of coastal watersheds: historical increases in nitrogen loads and eutrophication of Waquoit Bay estuaries. Can J Fish Aquat Sci 58:1489–1500

Bratton JF (2010) The three scales of submarine groundwater flow and discharge across passive continental margins. J Geol 118(5):565–575

Briggs RA, Ruttenberg KC, Ricardo AE, Glazer BT (2013) Constraining sources of organic matter to tropical coastal sediments: consideration of non-traditional end members. Aquat Geochem 19(5–6):543–563

Burnett WC, Dulaiova H (2003) Estimating the dynamics of groundwater input into the Coastal Zone via continuous Radon-222 measurements. J Environ Radioact 69(1–2):21–35

Charette MA (2007) Hydrologic forcing of submarine groundwater discharge: insight from a seasonal study of radium isotopes in a groundwater-dominated salt marsh estuary. Limnol Oceanogr 52(1):230–239

Charette MA, Sholkovitz ER, Hansel CM (2005) Trace element cycling in a subterranean estuary, part 1: geochemistry of the permeable sediments. Geochim Cosmochim Acta 69:2095–2109

Charette MA, Moore WS, Burnett WC (2008) Uranium- and thorium-series nuclides as tracers of submarine groundwater discharge. Radioact Environ 13:155–191

Cyronak T, Schulz KG, Santos IR, Eyre BD (2014) Enhanced acidification of global coral reefs driven by regional biogeochemical feedbacks. Geophys Res Lett 41(15):5538–5546

Dailer ML, Knox RS, Smith JE, Napier M, Smith CM (2010) Using δ15N values in algal tissue to map locations and potential sources of anthropogenic nutrient inputs on the island of Maui, Hawai'i, USA. Mar Pollut Bull 60:655–671

Dimova NT, Swarzenski PW, Dulaiova H, Glenn C (2012) Utilizing multi-channel electrical resistivity methods to examine the dynamics of the freshwater–saltwater interface in two Hawaiian groundwater systems. J Geophys Res 117. doi:10.1029/2011JC007509

Dollar SJ, Atkinson MJ (1992) Effects of nutrient subsidies from groundwater to near shore marine ecosystems off the island of Hawaii. Estuar Coast Shelf Sci 35:409–424

Drupp P, DeCarlo EH, Mackenzie FT, Bienfang P, Sabine CL (2011) Nutrient inputs, phytoplankton response, and CO2 variations in a semi-enclosed subtropical embayment, Kaneohe Bay, Hawaii. Aquat Geochem 17:473–498

Dulaiova H, Burnett WC, Wattayakorn G, Sojisuporn P (2006) Are the groundwater inputs into river-dominated areas important? The Chao Phraya River-Gulf of Thailand. Limnol Oceanogr 51:2232–2247

Dulaiova H, Camilli R, Henderson PB, Charette MA (2010) Coupled radon, methane and nitrate sensors for large-scale assessment of groundwater discharge and non-point source pollution to coastal waters. J Environ Radioact 101(7):553–563. doi:10.1016/j.jenvrad.2009.12.004

Garrison GH, Glenn CR, McMurtry GM (2003) Measurement of submarine groundwater discharge in Kahana Bay, Oahu, Hawaii. Limnol Oceanogr 48:920–928

Glenn CG, Whittier RB, Dailer ML, Dulaiova H, El-Kadi AI, Fackrell J, Kelly JL, Waters CA, Sevadjian J (2013) Lahaina groundwater tracer study—Lahaina, Maui, Hawaii. Final Report prepared for the State of Hawaii Department of Health, US EPA and US Army Engineer Research and Development Center. 502 pp

Gonneea ME, Charette MA (2014) Hydrologic controls on nutrient cycling in an unconfined coastal aquifer. Environ Sci Tech 48:14178–14185

Gonneea ME, Morris P, Dulaiova H, Charette MA (2008) New perspectives on radium behavior within a subterranean estuary. Mar Chem 109:250–267

Holleman K (2011) Comparison of submarine groundwater discharge, coastal residence times, and rates of primary productivity, Manualua Bay, Oahu and Honokohau Harbor, Big Island, Hawaii, USA. M.S. Thesis, University of Hawaii

Hoover DJ (2002) Fluvial nitrogen and phosphorus inputs to Hawaiian coastal waters: storm loading, particle-solution transformations and ecosystem impacts. Unpublished Ph.D. discussion, Department of Oceanography, University of Hawaii

Hoover DJ et al (2009) Fluvial Fluxes of water, suspended particulate matter, and nutrients and potential impacts on tropical coastal water biogeochemistry: Oahu, Hawaii. Aquat Geochem 15:547–570

Izuka SK, Hill BR, Shade PJ, Tribble GW (1994) Geohydrology and possible transport routes of polychlorinated biphenyls in Haiku valley, Oahu, Hawaii. Water-Resources Investigations Report 92-4168. U.S. Geological Survey

Johnson EE, Wiegner TN (2014) Surface water metabolism potential in groundwater-fed coastal waters of Hawaii Island, USA. Estuar Coasts 37:712–723. doi:10.1007/s12237-013-9708-y

Johnson AG, Glenn CR, Burnett WC, Peterson RN, Lucey PG (2008) Aerial infrared imaging reveals large nutrient-rich groundwater inputs to the ocean. Geophys Res Lett 35(15), L15606

Kaul LW, Froelich PN (1984) Modeling estuarine nutrient geochemistry in a simple system. Geochem Cosmochim Acta 48:1417–1433

Kelly RP, Moran SB (2002) Seasonal changes in groundwater input to a well-mixed estuary estimated using radium isotopes and implications for coastal nutrient budgets. Limnol Oceanogr 47:1796–1807

Kim G, Kim J-S, Hwang D-W (2011) Submarine groundwater discharge from oceanic islands standing in oligotrophic oceans: implications for global biological production. Limnol Oceanogr 56(2):673–682

Kim TH, Waska H, Kwon EH, Suryaputra IGN, Kim G (2012) Production, degradation, and flux of dissolved organic matter in the subterranean estuary of a large tidal flat. Mar Chem 142–144:1–10

Kiro Y, Weinstein Y, Starinsky A, Yechieli Y (2013) Groundwater ages and reaction rates during seawater circulation in the Dead Sea aquifer. Geochim Cosmochim Acta 122:17–35. doi:10.1016/j.gca.2013.08.005

Kleven A (2014) Coastal Groundwater Discharge as a Source of Nutrients to He'eia Fishpond, O'ahu, HI. Undergraduate thesis, Global Environmental Science Program, University of Hawaii at Manoa. XB-12-02

Knee KL, Street JH, Grossman EE, Boehm AB, Paytan A (2010) Nutrient inputs to the coastal ocean from submarine groundwater discharge in a groundwater-dominated system: relation to land use (Kona Coast, Hawai'i, USA). Limnol Oceanogr 55:1105–1122

Knee KL, Garcia-Solosna E, Garcia-Orellana J, Boehm AB, Paytan A (2011) Using radium isotopes to characterize water ages and coastal mixing rates: a sensitivity analysis. Limnol Oceanogr Methods 9:380–395

Krest JM, Moore WS, Rama (1999) ^{226}Ra and ^{228}Ra in the mixing zones of the Mississippi and Atchafalaya Rivers: indicators of groundwater input. Mar Chem 64:129–152

Kroeger KD, Charette MA (2008) Nitrogen biogeochemistry of submarine groundwater discharge. Limnol Oceanogr 53:1025–1039

Kwon EY, Kim G, Primeau F, Moore WS, Cho H-M, DeVries T, Sarmiento JL, Charette MA, Cho Y-K (2015) Global estimate of submarine groundwater discharge based on an observationally constrained radium isotope model. Geophys Res Lett 41:8438–8444. doi:10.1002/2014GL061574

Laws EA (1980) Effects of waste-water discharges on phytoplankton communities. In: University of Hawaii, Sea Grant Cooperative Report UNIHI-SEAGRANT-CR-80-1. pp. 13–40

Lee DR (1977) A device for measuring seepage flux in lakes and estuaries. Limnol Oceanogr 22:140–147

Leta OT, El-kadi A, Dulaiova H, Ghazal K (2015) Applicability of the SWAT model for hydrological modeling of a small-scale watershed in Hawaii under scarcity of hydrological data. J Hydrol Eng (in press)

Li HL, Jiao JJ (2013) Quantifying tidal contribution to submarine groundwater discharges: a review. Chin Sci Bull 58(25):3053–3059

Lowe R, Falter JL, Monismith SG, Atkinson MJ (2009) A numerical study of circulation in a coastal reef-lagoon system. J Geophys Res 114:C06022. doi:10.1029/2008JC005081

Lucas LV, Thompson JK, Brown LR (2009) Why are diverse relationships observed between phytoplankton biomass and transport time? Limnol Oceanogr 54(1):381–390

Maeda M, Windom HL (1982) Behavior of uranium in two estuaries of the south-eastern United States. Mar Chem 11:427–436

Mayfield KK (2013) A summary of the submarine groundwater discharge (SGD) in Kahana Bay: spatial and intra-daily variability. Undergraduate thesis, Global Environmental Science Program, University of Hawaii at Manoa. 48 p

Michael HA, Mulligan AE, Harvey CF (2005) Seasonal oscillations in water exchange between aquifers and the coastal ocean. Nature 436(7054):1145–1148

Moore WS (1996) Large groundwater inputs to coastal waters revealed by 226Ra enrichments. Nature 380:612–614

Moore WS (1997) The effects of groundwater input at the mouth of the Ganges-Brahmaputra Rivers on barium and radium fluxes to the Bay of Bengal. Earth Planet Sci Lett 150:141–150

Moore WS (1999) The subterranean estuary: a reaction zone of ground water and sea water. Mar Chem 65:111–126

Moore WS (2000a) Determining coastal mixing rates using radium isotopes. Cont Shelf Res 20:1993–2007

Moore WS (2000b) Ages of continental shelf waters determined from 223Ra and 224Ra. J Geophys Res 105:22117–22122

Moore WS (2003) Sources and fluxes of submarine groundwater discharge delineated by radium isotopes. Biogeochemistry 66:75–93

Moore WS (2006) The role of submarine groundwater discharge in coastal biogeochemistry. J Geochem Explor 88:389–393

Moore WS (2010) The effect of submarine groundwater discharge on the ocean. Ann Rev Mar Sci 2:59–88

Moore WS, Wilson AM (2005) Advective flow through the upper continental shelf driven by storms, buoyancy, and submarine groundwater discharge. Earth Planet Sci Lett 235:564–576

Moore WS, Blanton JO, Joye SB (2006) Estimates of flushing times, submarine groundwater discharge, and nutrient fluxes to Okatee Estuary, South Carolina. J Geophys Res 111. doi:10.1029/2007jc004199

Moore WS, Sarmiento JL, Key RM (2008) Submarine ground-water discharge revealed by 228Ra distribution in the upper Atlantic Ocean. Nat Geosci 1:309–311

Paytan A, Shellenbarger GG, Street JH, Gonneea ME, Davis K, Young MB, Moore WS (2006) Submarine groundwater discharge: an important source of new inorganic nitrogen to coral reef ecosystems. Limnol Oceanogr 51:343–348

Peterson PN, Burnett WC, Taniguchi M, Chen J, Santos IR, Ishitobi T (2009) Radon and radium isotope assessment of submarine groundwater discharge in the Yellow River delta, China. J Geophys Res 113:1–14

Ringuet S, Mackenzie FT (2005) Controls on nutrient and phytoplankton dynamics during normal flow and storm runoff conditions, southern Kaneohe Bay, Hawaii. Estuaries 28:327–337

Robinson C, Li L, Prommer H (2006) Tide-induced recirculation across the aquifer-ocean interface. Water Resour Res 43(7), W07428

Robinson C, Li L, Barry DA (2007) Effect of tidal forcing on a subterranean estuary. Adv Water Resour 30(4):851–865

Roy M, Martin JB, Cherrier J, Cable JE, Smith CG (2010) Influence of sea level rise on iron diagenesis in an east Florida subterranean estuary. Geochim Cosmochim Acta 74 (19):5560–5573

Santoro AE, Boehm AB, Francis CA (2006) Denitrifier community composition along a nitrate and salinity gradient in a coastal aquifer. Appl Environ Microbiol 72(3):2102–2109

Santos IR, Burnett WC, Chanton J, Suryaputra B, Dittmar T (2008) Nutrient biogeochemistry in a Gulf of Mexico subterranean estuary and groundwater-derived fluxes to the coastal ocean. Limnol Oceanogr 53(2):705–718

Santos IR, Eyre BD, Glud RN (2010) Influence of porewater advection on denitrification in carbonate sands: evidence from repacked sediment column experiments. Geochim Cosmochim Acta 96:247–258

Santos IR, Eyre BD, Huettel M (2012) The driving forces of porewater and groundwater flow in permeable coastal sediments: a review. Estuar Coast Shelf Sci 98:1–15

Santos IR, Glud RN, Maher D, Erler D, Eyre BD (2013) Diel coral reef acidification driven by porewater advection in permeable carbonate sands, Heron Island, Great Barrier Reef. Geophys Res Lett 38(3)

Schoelynck J, Bal K, Backx H, Okruszko T, Meire P, Struyf E (2010) Silica uptake in aquatic and wetland macrophytes: a strategic choice between silica, lignin and cellulose? New Phytol 186 (2):385–391

Shade PJ, Nichols WD (1996). Water budget and the effects of land-use changes on ground-water recharge, Oahu, Hawaii. USGS Professional Paper 1412-C

Slomp CP, Van Cappellen P (2004) Nutrient inputs to the coastal ocean through submarine groundwater discharge: controls and potential impact. J Hydrol 295:64–86

Smith SV, Kimmerer W, Laws E, Brock RE, Walsh T (1981) Kaneohe Bay sewage diversion experiment: perspectives on ecosystem responses to nutritional perturbation. Pac Sci 35(4)

Smith J, Smith C, Hunter C (2001) An experimental analysis of the effects of herbivory and nutrient enrichment on benthic community dynamics on a Hawaiian reef. Coral Reefs 19(4):332–342

Spiteri C, Slomp CP, Charette MA, Tuncay K, Meile C (2008) Flow and nutrient dynamics in a subterranean estuary (Waquoit Bay, MA, USA): field data and reactive transport modeling. Geochim Cosmochim Acta 72:3398–3412

Street JH, Knee KL, Grossman EE, Paytan A (2008) Submarine groundwater discharge and nutrient addition to the coastal zone and coral reefs of leeward Hawai. Mar Chem 109:355–376

Taniguchi M, Burnett WC, Cable JE, Turner JV (2002) Investigation of submarine groundwater discharge. Hydrol Process 16:2115–2129

Taniguchi M, Burnett WC, Smith CF, Paulsen RJ, O'Rourke D, Krupa SL, Christoff JL (2003) Spatial and temporal distributions of submarine groundwater discharge rates obtained from various types of seepage meters at a site in the Northeastern Gulf of Mexico. Biogeochemistry 66:35–53

Timmerman A, Young C, McManus MA, Ruttenberg KC, D'Andrea B (2015). Seasonal dynamics of freshwater input to a tropical coastal marine embayment. Estuar Coast Shelf Sci

Tomasky G, Valiela I, Charette MA (2013) Determination of water mass ages using radium isotopes as tracers: implications for phytoplankton dynamics in estuaries. Mar Chem 156:18–26

Wang G, Wang Z, Zhai W, Moore WS, Li Q, Yan X, Qi D, Jiang Y (2014) Net subterranean estuarine export fluxes of dissolved inorganic C, N, P, Si, and total alkalinity into the Jiulong River estuary, China. Geochim Cosmochim Acta 149:103–114

Wankel SD, Kendall C, Paytan A (2009) Using nitrate dual isotopic composition (dN and dO) as a tool for exploring sources and cycling of nitrate in an estuarine system: Elkhorn Slough, California. J Geophys Res 114:G01011. doi:10.1029/2008JG000729

Waska H, Kim G (2011) Submarine groundwater discharge (SGD) as a main nutrient source for benthic and water-column primary production in a large intertidal environment of the Yellow Sea. J Sea Res 65:103–113

Weston NB, Porubsky WP, Samarkin V, MacAvoy S, Erickson M, Joye SB (2006) Pore water stoichiometry of terminal metabolic products, sulfate, and dissolved organic carbon and nitrogen in intertidal creek-bank sediments. Biogeochemistry 77:375–408

Wilson AM, Gardner LR (2006) Tidally driven groundwater flow and solute exchange in a marsh: numerical simulations. Water Resour Res 42:W01405. doi:10.1029/2005WR004302

Windom HL, Moore WS, Niecheski LFH, Jahnke R (2006) Submarine groundwater discharge: a large, previously unrecognized source of dissolved iron to the South Atlantic Ocean. Mar Chem 102:252–266

Young CW (2011) Perturbation of nutrient inventories and phytoplankton community composition during storm events in a tropical coastal system: He'eia Fishpond, O'ahu, Hawaii. M.S. Thesis, The Department of Oceanography, University of Hawaii, 400 pp

Zektser IS (2000) Groundwater and the environment: applications for the global community. Lewis Publishers (CRC Press LLC)